# $Cos(2\phi_h)$ asymmetry in $J/\psi$ production in unpolarized $ep$ collision

Raj Kishore, Asmita Mukherjee, and Mariyah Siddiqah
*Department of Physics, Indian Institute of Technology Bombay, Mumbai-400076, India*

(Received 24 March 2021; accepted 7 October 2021; published 10 November 2021)

We present a calculation of the $\cos(2\phi_h)$ asymmetry in $J/\psi$ production in electron-proton collisions at the future electron-ion collider (EIC), a useful channel to probe the transverse momentum dependent gluon distribution functions also known as gluon transverse momentum dependent parton distributions (TMDs). The dominant subprocess for the $J/\psi$ production is the virtual-photon-gluon fusion process $\gamma^* + g \to J/\psi + g$. The production of $J/\psi$ is calculated in the nonrelativistic quantum chromodynamics framework with the inclusion of both color singlet and color octet contributions. Numerical estimates of the $\cos(2\phi_h)$ asymmetry are given in the kinematical region to be accessed by the future EIC. The asymmetry depends on the parametrization of the gluon TMDs, as well as on the long distance matrix elements. We use both Gaussian-type parametrization and the McLerran-Venugopalan model for the TMDs in the kinematical region of small $x$, where the gluons play a dominant role. The asymmetry may be useful to probe the ratio of the linearly-polarized and the unpolarized gluon distribution in the proton.

DOI: 10.1103/PhysRevD.104.094015

## I. INTRODUCTION

Quantum chromodynamics (QCD) is an exceptionally rich and complex theory of strong interactions between quarks and gluons, the fundamental constituents of matter. However, these quarks and gluons do not exist in nature as free particles but are confined inside hadrons, and their fundamental properties can be explored only with the help of scattering processes. The hadron physics community has expanded its inquiry beyond the ordinary one-dimensional collinear parton distribution functions (PDFs) in the motion of the parton and its spatial distribution in a direction perpendicular to the momentum of the parent hadron.

To account for transverse motion, the collinear PDFs were extended to transverse-momentum-dependent PDFs, also referred to as transverse momentum dependent parton distributions (TMDs)[1–3]. TMDs have attracted an enormous amount of interest and are being investigated at the current facilities including JLAB 12 GeV upgrade, RHIC, and are planned to be investigated at the future electron-ion collider (EIC). TMDs are considered as an extension of the standard, one-dimensional PDFs to the three-dimensional momentum space. Due to the gauge invariance, the operator definition of TMDs requires the inclusion of gauge links or Wilson lines. Unlike collinear PDFs, which are universal, TMDs are process dependent due to their initial and final state interactions [4,5], or the gauge links. In other words, the TMDs extracted from semi-inclusive deep inelastic scattering (SIDIS) are not the same as extracted from Drell-Yan processes due to the difference in gauge links. TMDs are sensitive to the soft gluon exchanges and the color flow in the specific sub-processes in which they are probed. SIDIS and Drell-Yan processes provide the majority of experimental data for the extraction of TMDs, where the observables of interest are the single-spin asymmetries and azimuthal asymmetries, which have been measured and are currently under direct experimental scrutiny [6–8].

A lot of work has recently been done to extract quark TMDs inside a proton from low-energy data from HERMES, COMPASS, or JLab experiments. Contrarily, little is experimentally known about the gluon TMDs [9], as they typically require higher-energy scattering processes and are harder to isolate in comparison to quark TMDs. Each gluon TMD contains multiple gauge links while the quark TMDs contain one, due to which the process dependence of gluon TMDs is more involved than quark TMDs [10]. Gluon TMDs parametrize the transverse motion of gluons inside a proton. In the parton model, the gluon correlator of the unpolarized spin-1/2 hadron is parametrized in terms of leading twist distribution functions [9] $i.e. f_1^g(x, \mathbf{k}_\perp^2)$ and $h_1^{\perp g}(x, \mathbf{k}_\perp^2)$. The function $f_1^g(x, \mathbf{k}_\perp^2)$ represents the probability of finding an unpolarized gluon, within an unpolarized hadron, with a longitudinal momentum fraction $x$ and transverse momentum $k_\perp$, while $h_1^{\perp g}(x, \mathbf{k}_\perp^2)$ represents the distribution of linearly-polarized gluons within the unpolarized hadron

and is also known as Boer-Mulders function. These are the only two TMDs of the unpolarized proton that provide essential knowledge on the transverse dynamics of the gluon content of the proton. They are also important for the proper explanation of gluon-fusion processes at all energies. At small $x$, it turns out that the linearly-polarized distribution may reach its maximally allowed size, bounded by the unpolarized gluon density [9]. Depending on the gauge links, there are two types of gluon TMDs, Weizsäcker-Williams (WW) type where both gauge links are either future or past pointing [11,12], and dipole type where one gauge link is future pointing and one past [13]. $ep$ collision probes the WW type gluon distribution. Various methods have been proposed to measure both $f_1^g(x, \mathbf{k}_\perp^2)$ and $h_1^{\perp g}(x, \mathbf{k}_\perp^2)$, as well as other gluon TMDs, for example [10,14–34].

In the last few years, the distribution of linearly-polarized gluons within an unpolarized proton has attracted a lot of interest; as yet they have not been extracted experimentally. A lot of theoretical investigations has been put forward to probe $h_1^{\perp g}(x, \mathbf{k}_\perp^2)$, and a model-independent theoretical upper bound can be found in Ref. [9,35]. They are time-reversal even (T even) objects, affecting the unpolarized cross section of scattering processes, as well as an azimuthal asymmetry of the type $\cos(2\phi_h)$ [36]. Processes like heavy quark pair or dijet production in SIDIS [36], and diphoton pair [16] and $\Upsilon(1S) + \text{jet}$ [37] production in $pp$ collision have been suggested for extracting $h_1^{\perp g}(x, \mathbf{k}_\perp^2)$. It has been seen in these processes that $h_1^{\perp g}(x, \mathbf{k}_\perp^2)$ can be probed by measuring azimuthal asymmetries. It can also be probed in heavy quark pair production in lepton-proton and proton-proton collisions [36,38,39],as well as associated production of dilepton and $J/\psi$ [25]. Quarkonium production is a useful tool to probe the gluon TMDs (see [40] for a recent review). $J/\psi$ production in SIDIS is a good channel, as the effect of the gauge links is simpler compared to $pp$ collisions, and one can assume the generalized factorization. Quite a lot of theoretical work has been done recently in this direction. TMDs can be accessed through this process when the transverse momentum of the produced $J/\psi$ ($P_{h\perp}$) is not very large, $|P_{h\perp}| < M$, where $M$ is the mass of $J/\psi$. This kinematical region is expected to be accessible at the future EIC.

In Ref. [22] the authors proposed a method to probe $h_1^{\perp g}$ by studying the $\cos(2\phi_h)$ asymmetry in $J/\psi$ production through the leading-order (LO) process $\gamma^* + g \to J/\psi$ at the future EIC. This receives contribution at LO at $z = 1$, where $z$ is the fraction of photon energy transferred to $J/\psi$. In Ref. [30] the $\cos(2\phi_h)$ asymmetry was calculated in the process $e(l) + p(P) \to e(l') + J/\psi(P_h) + X(P_x)$, in the kinematical region $z < 1$, which includes contributions at next-to-leading order (NLO). To simplify the calculation, only color singlet (CS) contributions in the nonrelativistic quantum chromodynamics (NRQCD) framework were included, and the small-$x$ region was explored. The asymmetry was found to be rather small, and the contribution to the asymmetry came mainly from one Feynman diagram. Nevertheless, it was possible to disentangle $h_1^{\perp g}$ and the unpolarized gluon TMD and the numerator of the asymmetry was found to be dependent only on $h_1^{\perp g}$. As we know, the color octet contributions are important in NRQCD formulation in the production of $J/\psi$ [27]. In this work, we extend our study to investigate the $\cos(2\phi_h)$ asymmetry in the above process, but taking into account also the color octet (CO) contributions in NRQCD; which makes the calculation rather lengthy. We explore the small-$x$ region, where the gluon TMDs play an important role.

NRQCD is an effective field theory approach, in which the production cross section can be written in a factorized form into a perturbative hard part where the quarks and gluons form the heavy-quark and antiquark pair, which may be in the CS or the CO state, and a nonperturbative soft part where the heavy quark pair forms a bound state. All the information of hadronization of the heavy quark pair is encoded in the long-distance matrix elements (LDME), which are usually extracted by fitting experimental data. They describe the transition probability to form the quarkonium state from the heavy quark pair. LDMEs are expected to scale with a definite power of the heavy quark velocity parameter $v$ in the limit $v \ll 1$. Thus NRQCD introduces an expansion both in $\alpha_s$ as well as in $v$, with $v^2 \approx 0.3$ for charmonium and $v^2 \approx 0.1$ for bottomonium. Thus, one has to consider all the Fock states of the heavy quark pair, $Q\bar{Q}$, produced in the hard scattering. Each Fock state is denoted by $n = {}^{2S+1}L_J^{[a]}$, where $J$, $L$, and $S$ are total angular momentum, orbital angular momentum, and spin quantum numbers, respectively, and $a$ is the color multiplicity carrying a value of 1 for color singlet and 8 for color octet state. For the $J/\psi$ $S$-wave quarkonium state, the dominant contribution in NRQCD in the limit $v \to 0$ reduces to a color-singlet model (CSM), where the heavy quark pair is directly produced in a CS state, having the same quantum numbers as that of the $J/\psi$. A $Q\bar{Q}$ pair produced in the color octet state with different quantum numbers eventually evolves into the physical color singlet quarkonia by the emission of soft gluons [40].

A good description of $J/\psi$ by NRQCD is given at RHIC energies [41]. Azimuthal asymmetries in $J/\psi$ production in these processes may also be used as a tool to get information on the LDMEs in NRQCD [42]. In our study of $\cos(2\phi_h)$ azimuthal asymmetry in $J/\psi$, we will use the NRQCD formalism. We will take the dominant $\gamma^* + g \to J/\psi + g$ partonic subprocess into consideration, and investigate mainly the small-$x$ region, where the gluon TMDs play a very important role.

The rest of this paper is organized as follows. The analytical framework of our calculation is discussed in

Sec. II. In Sec. III, we present our numerical results and finally, in Sec. IV, we conclude.

## II. AZIMUTHAL ASYMMETRY IN $J/\psi$ LEPTOPRODUCTION

### A. Calculation of the cross section and asymmetry

We consider semi-inclusive production of $J/\psi$ in unpolarized $ep$ collision

$$e(l) + p(P) \to e(l') + J/\psi(P_h) + X(P_x), \tag{1}$$

where the quantities within the brackets are the four-momentum of corresponding particles and $X$ represents the proton remnant. We use the following invariants to describe the kinematics of this process,

$$Q^2(=-q^2), \qquad W^2 = (P+q)^2, \qquad z = \frac{P\cdot P_h}{P\cdot q}. \tag{2}$$

The other two dimensionless invariants are

$$y = \frac{P\cdot q}{P\cdot l}, \qquad x_B = \frac{Q^2}{2P\cdot q}. \tag{3}$$

The quantity $Q^2$ is the virtuality of the photon, $W^2$ is the invariant mass squared of the virtual photon-target system, $z$ is the fraction of energy transferred from the photon to $J/\psi$ in the frame where the initial proton is at rest, $y$ is the inelasticity variable and has a physical interpretation as the fraction of the energy of the electron transferred to the proton. The variable $x_B(=Q^2/2P\cdot q)$ is known as Bjoken-$x$.

To study the azimuthal asymmetry, we use a frame in which the incoming proton and the virtual photon exchanged in the process move in $+z$ and $-z$ directions. The kinematics here is defined in terms of two lightlike vectors with the help of a Sudakov decomposition, chosen here to be the momentum $P(=n_-)$ of the incoming proton, and a second vector $n(=n_+)$, obeying the relations $n\cdot P = 1$ and $n_+^2 = n_-^2 = 0$. Thus one can have the following expressions for the momenta of the incoming proton and virtual photon $(q = l - l')$

$$P = n_- + \frac{M_p^2}{2}n_+ \approx n_-, \tag{4}$$

$$q = -x_B n_- + \frac{Q^2}{2x_B}n_+ \approx -x_B P + (P\cdot q)n_+, \tag{5}$$

where $M_p$ is the mass of proton. Moreover, the momenta of incoming and outgoing lepton can be written as

$$\begin{aligned} l &= \frac{1-y}{y}x_B P + \frac{1}{y}\frac{Q^2}{2x_B}n + \frac{\sqrt{(1-y)}}{y}Q\hat{l}_\perp \\ &= \frac{1-y}{y}x_B P + \frac{s}{2}n + \frac{\sqrt{(1-y)}}{y}Q\hat{l}_\perp, \end{aligned} \tag{6}$$

$$\begin{aligned} l' &= \frac{1}{y}x_B P + \frac{1-y}{y}\frac{Q^2}{2x_B}n + \frac{\sqrt{(1-y)}}{y}Q\hat{l}_\perp \\ &= \frac{1}{y}x_B P + (1-y)\frac{s}{2}n + \frac{\sqrt{(1-y)}}{y}Q\hat{l}_\perp. \end{aligned} \tag{7}$$

Here $s = (l+P)^2 = 2P\cdot l$ is the squared center of mass energy of the electron-proton scattering and $Q^2, s, y$, and $x_B$ are related by the relation $Q^2 = s x_B y$. At leading order, $J/\psi$ is produced by the virtual-photon gluon fusion for which $z = 1$ [22]. Since at small $x$ the proton is rich in gluons, the dominant subprocess for the $J/\psi$ production is the virtual-photon-gluon fusion process $\gamma^*(q) + g(k) \to J/\psi(P_h) + g(p_g)$. In terms of the lightlike vectors defined above the four-momentum of the initial state gluon, the final state gluon, and $J/\psi$ are expressed as

$$k = xP + k_\perp + (k\cdot P - xM_p^2)n \approx xP + k_\perp, \tag{8}$$

$$p_g = (1-z)(P\cdot q)n + \frac{\mathbf{p}_{g\perp}^2}{2(1-z)P\cdot q}P + p_{g\perp}, \tag{9}$$

$$P_h = z(P\cdot q)n + \frac{M^2 + \mathbf{P}_{h\perp}^2}{2zP\cdot q}P + P_{h\perp}. \tag{10}$$

Here $x = k\cdot n$ is the light-cone momentum fraction of the gluon, $M$ is the mass of $J/\psi$ and $P_h^2 = -\mathbf{P}_{h\perp}^2$. The Mandelstam variables for the partonic subprocess $\gamma^*(q) + g(k) \to J/\psi(P_h) + g(p_g)$ become

$$\begin{aligned} \hat{s} &= (k+q)^2 = q^2 + 2k\cdot q = \frac{xQ^2}{x_B} - Q^2, \\ \hat{t} &= (t - P_h)^2 = M^2 - 2k\cdot P_h \\ &= M^2 - \frac{xzQ^2}{x_B} + 2k_\perp P_{h\perp}\cos(\phi - \phi_h), \\ \hat{u} &= (q - P_h)^2 = M^2 + q^2 - 2q\cdot P_h \\ &= M^2 - (1-z)Q^2 - \frac{M^2 + P_{h\perp}^2}{z}, \end{aligned}$$

where $\phi$ and $\phi_h$ represent the azimuthal angles of initial gluon and the transverse momentum of $J/\psi$, respectively. Due to the presence of the gauge links or initial/final state interactions, factorization in many of such processes are still not proven. However, $ep$ collision processes are less complicated than $pp$ collisions in terms of color flow, and factorization is expected to hold. In [43] the process

$ep \to e + J/\psi + X$ is compared with the SIDIS, for which TMD factorization has been proven. It is argued that the additional scale, namely, the mass of $J/\psi$ does not affect the gauge link structure, and TMD factorization is expected to be valid for this process as well. Following the approach of Refs. [22,44], we assume the generalized factorization in the kinematics considered. Also to be noted is that we have considered only one subprocess in our calculation, which is dominating in the kinematical region of our interest. A complete NLO calculation in QCD needs to take into account all partonic subprocesses, both for real emission as well as virtual diagrams; the effect of the soft functions in the correlators, and effect of soft gluon emission in the LDMEs, or the shape functions [43] at this order. Only then are the singularities expected to cancel systematically and a finite result can be obtained. The aim of this work is to explore the phenomenology related to probing the TMDs in this process in a given kinematical region accessible in experiments, for example at the future EIC. As discussed later, we have imposed kinematical cuts to exclude the region where such divergences occur; the cuts that we have proposed can be realized in experiments.

The differential scattering cross section can be written as a convolution of leptonic tensor, a soft parton correlator for the incoming hadron and a hard part,

$$\begin{aligned} d\sigma = & \frac{1}{2s}\frac{d^3l'}{(2\pi)^3 2E_l'}\frac{d^3P_h}{(2\pi)^3 2E_{P_h}} \\ & \times \int \frac{d^3p_g}{(2\pi)^3 2E_g}\int dx d^2\mathbf{k}_\perp (2\pi)^4 \delta(q+k-P_h-p_g) \\ & \times \frac{1}{Q^4}\mathcal{L}^{\mu\mu'}(l,q)\Phi^{\nu\nu'}(x,\mathbf{k}_\perp)\mathcal{M}_{\mu\nu}(\mathcal{M}_{\mu'\nu'})^*. \end{aligned} \tag{11}$$

The term $\mathcal{M}_{\mu\nu}$ represents the amplitude of $J/\psi$ production in the $\gamma^* + g \to J/\psi + g$ partonic subprocess. The leptonic tensor is given by

$$\mathcal{L}^{\mu\mu'}(l,q) = e^2(-g^{\mu\mu'}Q^2 + 2(l^\mu l'^{\mu'} + l^{\mu'} l'^{\mu})), \tag{12}$$

where $e$ is the electronic charge. At leading twist, the gluon correlator of the unpolarized proton contains two TMD gluon distribution functions

$$\begin{aligned} \Phi_g^{\nu\nu'}(x,\mathbf{k}_\perp) = -\frac{1}{2x}\Bigg\{ & g_\perp^{\nu\nu'} f_1^g(x,\mathbf{k}_\perp^2) \\ & - \left(\frac{k_\perp^\nu k_\perp^{\nu'}}{M_p^2} + g_\perp^{\nu\nu'}\frac{\mathbf{k}_\perp^2}{2M_p^2}\right) h_1^{\perp g}(x,\mathbf{k}_\perp^2)\Bigg\}, \end{aligned} \tag{13}$$

where $g_\perp^{\nu\nu'} = g^{\nu\nu'} - P^\nu n^{\nu'}/P\cdot n - P^{\nu'} n^\nu / P\cdot n$. The quantities $f_1^g(x,\mathbf{k}_\perp^2)$ and $h_1^{\perp g}(x,\mathbf{k}_\perp^2)$ represent the unpolarized and the linearly-polarized gluon distribution functions respectively.

### B. $J/\psi$ production in NRQCD based color-octet model

The amplitude for the production of $J/\psi$ can be written as follows [44,45]:

$$\begin{aligned} & \mathcal{M}(\gamma^* g \to Q\bar{Q}[^{2S+1}L_J^{(1,8)}](P_h) + g) \\ & = \sum_{L_z S_z}\int \frac{d^3\mathbf{k}'}{(2\pi)^3}\Psi_{LL_z}(\mathbf{k}')\langle LL_z; SS_z|JJ_z\rangle \\ & \quad \mathrm{Tr}[O(q,k,P_h,k')\mathcal{P}_{SS_z}(P_h,k')]. \end{aligned} \tag{14}$$

We have suppressed the indices $\mu$, $\nu$ in $\mathcal{M}$ and in $O(q,k,P_h,k')$. Here $\Psi_{LL_z}(\mathbf{k}')$ is the nonrelativistic bound-state wave function with orbital angular momentum $L, L_z$ and the relative momentum $k'$ of the heavy quark in the quarkonium rest frame; $k'$ is assumed to be smaller than $P_h$. $\langle LL_z; SS_z|JJ_z\rangle$ are the usual Clebsch-Gordan coefficients, $O(q,k,P_h,k')$ represents the amplitude for the production of the heavy quark pair $Q\bar{Q}$ and is calculated from the Feynman diagrams. The Feynman diagrams relevant for this process are given in Fig. 1. The polarization vectors of the initial gluons and the heavy quark-antiquark legs are absorbed into the definitions of the gluon correlators and in the bound-state wave function, respectively. The quantity

$$\begin{aligned} \mathcal{P}_{SS_z}(P_h,k') &= \sum_{s_1,s2}\left\langle \frac{1}{2}s_1;\frac{1}{2}s_2|SS_z\right\rangle v\left(\frac{P_h}{2}-k',s_1\right)\bar{u}\left(\frac{P_h}{2}+k',s_2\right) \\ &= \frac{1}{4M^{3/2}}(-\not{P}_h + 2\not{k}' + M)\Pi_{SS_z}(\not{P}_h + 2\not{k}' + M) + \mathcal{O}(k'^2), \end{aligned} \tag{15}$$

plays the role of spin projection operator [44,45] with

$$\Pi_{SS_z} = \begin{cases} \gamma_5, & \text{for singlet state } (S=0) \\ \not{\varepsilon}_{S_z}(P_h), & \text{for triplet state } (S=1), \end{cases}$$

where $\varepsilon_{S_z}(P_h)$ is the spin vector of the $Q\bar{Q}$ system. We consider here $\gamma^* + g \to J/\psi + g$, which is the dominating partonic subprocess.

By considering the contribution from all the above Feynman diagrams we can write the amplitude as

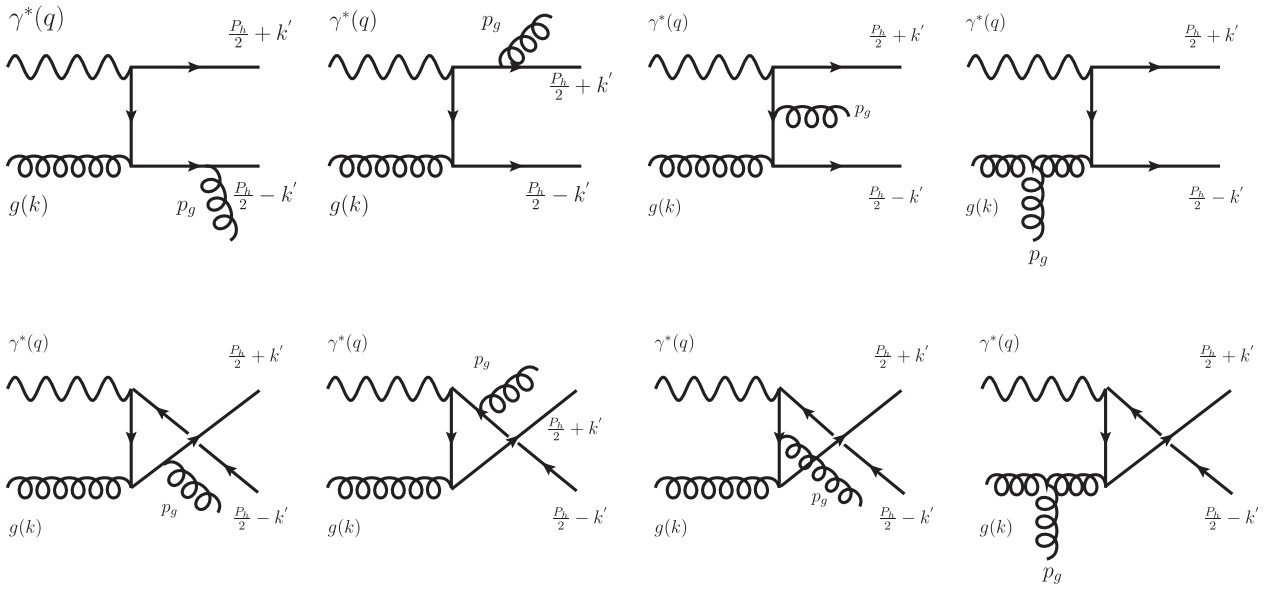


FIG. 1. Feynman diagrams for the partonic subprocess $\gamma^* + g \to J/\psi + g$.

$$O(q,k,P_h,k') = \sum_{m=1}^{8} \mathcal{C}_m O_m(q,k,P_h,k'), \tag{16}$$

where $\mathcal{C}_m$ represents the color factor of each diagram

$$\mathcal{C}_1 = \mathcal{C}_6 = \mathcal{C}_7 = \sum_{ij} \langle 3i;\bar{3}j|8c\rangle (t_a t_b)_{ij},$$
$$\mathcal{C}_2 = \mathcal{C}_3 = \mathcal{C}_5 = \sum_{ij} \langle 3i;\bar{3}j|8c\rangle (t_b t_a)_{ij},$$
$$\mathcal{C}_4 = \mathcal{C}_8 = \sum_{ij} \langle 3i;\bar{3}j|8c\rangle i f_{abd} (t_d)_{ij},$$

where the summation runs over the colors of the outgoing quark and antiquark. The $SU(3)$ Clebsch-Gordan coefficients for color singlet and color octet states, respectively, are given as

$$\langle 3i;\bar{3}j|1\rangle = \frac{\delta_{ij}}{\sqrt{N_c}}, \qquad \langle 3i;\bar{3}j|8a\rangle = \sqrt{2}(t^a)^{ij},$$

and they project out the color state of the $Q\bar{Q}$ pair either in the color singlet or in the color octet state. Here, $N_c$ represents the number of colors. In the fundamental representation the generators of the $SU(3)$ group is denoted by $t_a$ following which $\mathrm{Tr}(t_a t_b) = \delta_{ab}/2$ and $\mathrm{Tr}(t_a t_b t_c) = 1/4(d_{abc} + i f_{abc})$. In case of the color octet state, the color factors for the production of initial $Q\bar{Q}$ are

$$\mathcal{C}_1 = \mathcal{C}_6 = \mathcal{C}_7 = \frac{\sqrt{2}}{4}(d_{abc} + i f_{abc}),$$
$$\mathcal{C}_2 = \mathcal{C}_3 = \mathcal{C}_5 = \frac{\sqrt{2}}{4}(d_{abc} - i f_{abc}),$$
$$\mathcal{C}_4 = \mathcal{C}_8 = \frac{\sqrt{2}}{2} i f_{abc}.$$

The amplitudes $O_m(q,k,P_h,k')$ for the above Feynman diagrams are written as

$$O_1 = 4g_s^2 (ee_c)\varepsilon^{\rho *}_{\lambda_g}(p_g)\gamma_\nu \frac{\not{P}_h + 2\not{k}' - 2\not{q} + M}{(P_h + 2k' - 2q)^2 - M^2}\gamma_\mu \frac{-\not{P}_h + 2\not{k}' - 2\not{p}_g + M}{(P_h - 2k' + 2p_g)^2 - M^2}\gamma_\rho, \tag{17}$$

$$O_2 = 4g_s^2 (ee_c)\varepsilon^{\rho *}_{\lambda_g}(p_g)\gamma_\rho \frac{\not{P}_h + 2\not{k}' + 2\not{p}_g + M}{(P_h + 2k' + 2p_g)^2 - M^2}\gamma_\nu \frac{-\not{P}_h + 2\not{k}' + 2\not{k} + M}{(P_h - 2k' - 2k)^2 - M^2}\gamma_\mu, \tag{18}$$

$$O_3 = 4g_s^2 (ee_c)\varepsilon^{\rho *}_{\lambda_g}(p_g)\gamma_\nu \frac{\not{P}_h + 2\not{k}' - 2\not{q} + M}{(P_h + 2k' - 2q)^2 - M^2}\gamma_\rho \frac{-\not{P}_h + 2\not{k}' + 2\not{k} + M}{(P_h - 2k' - 2k)^2 - M^2}\gamma_\mu, \tag{19}$$

$$O_4 = 2g_s^2 (ee_c)\varepsilon^{\rho *}_{\lambda_g}(p_g)\gamma_\nu \frac{\not{P}_h + 2\not{k}' - 2\not{q} + M}{(P_h + 2k' - 2q)^2 - M^2}\gamma_\sigma \frac{1}{(k - p_g)^2}\mathcal{T}_{\mu\rho\sigma}(k, p_g), \tag{20}$$

where $M = 2m_c$, with $m_c$ representing the charm quark mass, and the tensor $\mathcal{T}_{\mu\rho\sigma}(k, p_g) = g_{\mu\rho}(k + p_g)_\sigma + g_{\rho\sigma}(k - 2p_g)_\mu + g_{\sigma\mu}(p_g - 2k)_\rho$ is the three gluon vertex. As all the Feynman diagrams are symmetric we can obtain the remaining four amplitudes $O_5$, $O_6$, $O_7$, and $O_8$ by reversing the fermion flow and replacing $k'$ by $-k'$. In the rest frame of the bound state, the relative momentum of $k'$ is very small as compared to $P_h$, thus Taylor expansion can be performed in powers of $k'$ around $k' = 0$ in Eq. (14). So it becomes convenient to split the radial and angular parts of the Fourier transformation of the wave function $\Psi_{LL_z}(\mathbf{k}')$,

$$\int \frac{d^3\mathbf{k}'}{(2\pi)^3} e^{i\mathbf{k}'.\mathbf{r}} \Psi_{LL_z}(\mathbf{k}') = \tilde{\Psi}_{LL_z}(\mathbf{r}) = R_L(|r|) Y_{LL_z}(\theta, \varphi),$$

where $\mathbf{r} = (|\mathbf{r}|, \theta, \varphi)$ in spherical coordinates, and $R_L(|r|)$ and $Y_{LL_z}(\theta, \varphi)$ are the radial wave function and spherical harmonic, respectively. In particular this means,

$$\int \frac{d^3\mathbf{k}'}{(2\pi)^3} \Psi_{00}(\mathbf{k}') = \frac{1}{\sqrt{4\pi}} R_0(0). \tag{21}$$

As the first term of the Taylor expansion at $\mathbf{k}' = 0$ does not depend on $\mathbf{k}'$ anymore, it gives the contribution from $S$ waves $(L = 0, J = 0, 1)$,

$$\mathcal{M}[^{2S+1}S_J^{(8)}](P_h, k) = \frac{1}{\sqrt{4\pi}} R_0(0) \mathrm{Tr}[O(q, k, P_h, k') \mathcal{P}_{SS_z}(P_h, k')]|_{k'=0} = \frac{1}{\sqrt{4\pi}} R_0(0) \mathrm{Tr}[O(0) \mathcal{P}_{SS_z}(0)], \tag{22}$$

where $O(0) = (q, k, P_h, 0)$ and $\mathcal{P}_{SS_z}(0) = \mathcal{P}_{SS_z}(P_h, 0)$. For $P$ waves $(L = 1, J = 0, 1, 2)$, $R_1(0) = 0$, so in the Taylor expansion the terms linear in $k^\alpha$ are considered in Eq. (14). Thus,

$$\int \frac{d^3\mathbf{k}'}{(2\pi)^3} k^\alpha \Psi_{1L_z}(\mathbf{k}) = -i\varepsilon^\alpha_{L_z}(P_h) \sqrt{\frac{3}{4\pi}} R_1'(0), \tag{23}$$

where $\varepsilon^\alpha_{L_z}(P_h)$ is a polarization vector for $L = 1$ bound state, and $R_1'(0)$ represents the derivative of the $P$-wave (radial) wave function evaluated at origin. Thus

$$\begin{aligned}\mathcal{M}[^{2S+1}P_J^{(8)}] &= -i\sqrt{\frac{3}{4\pi}} R_1'(0) \sum_{L_z S_z} \varepsilon^\alpha_{L_z}(P_h) \langle LL_z; SS_z | JJ_z \rangle \frac{\partial}{\partial k'^\alpha} \mathrm{Tr}[O(q, k, P_h, k') \mathcal{P}_{SS_z}(P_h, k')]|_{k'=0} \\ &= -i\sqrt{\frac{3}{4\pi}} R_1'(0) \sum_{L_z S_z} \varepsilon^\alpha_{L_z}(P_h) \langle LL_z; SS_z | JJ_z \rangle \mathrm{Tr}[O_\alpha(0) \mathcal{P}_{SS_z}(0) + O(0) \mathcal{P}_{SS_z\alpha}(0)],\end{aligned} \tag{24}$$

where

$$O_\alpha(0) = \frac{\partial}{\partial k'^\alpha} O(q, k, P_h, k')|_{k'=0},$$
$$\mathcal{P}_{SS_z\alpha}(0) = \frac{\partial}{\partial k'^\alpha} \mathcal{P}_{SS_z}(P_h, k')|_{k'=0}.$$

For $P$-waves we could utilize the following relations for Clebsch-Gordan coefficients and various polarisation vectors [46,47]

$$\sum_{L_z S_z} \langle 1L_z; SS_z | 00 \rangle \varepsilon^\alpha_{s_z}(P_h) \varepsilon^\beta_{L_z}(P_h) = \sqrt{\frac{1}{3}} \left( g^{\alpha\beta} - \frac{1}{M^2} P_h^\alpha P_h^\beta \right), \tag{25}$$

$$\sum_{L_z S_z} \langle 1L_z; 1S_z | 1J_z \rangle \varepsilon^\alpha_{s_z}(P_h) \varepsilon^\beta_{L_z}(P_h) = -\frac{i}{M} \sqrt{\frac{1}{2}} \epsilon_{\delta\lambda\rho\sigma} g^{\rho\alpha} g^{\sigma\beta} P_h^\delta \varepsilon^\lambda_{J_z}(P_h), \tag{26}$$

$$\sum_{L_z S_z} \langle 1L_z; 1S_z | 2J_z \rangle \varepsilon^\alpha_{s_z}(P_h) \varepsilon^\beta_{L_z}(P_h) = \varepsilon^{\alpha\beta}_{J_z}(P_h), \tag{27}$$

where the term $\varepsilon^\alpha_{J_z}(P_h)$ represents the polarization vector of bound state with $J = 1$, obeying the following relations

$$\varepsilon^\alpha_{J_z}(P_h) P_{h\alpha} = 0,$$
$$\sum_{L_z} \varepsilon^\alpha_{J_z}(P_h) \varepsilon^{*\beta}_{J_z}(P_h) = -g^{\alpha\beta} + \frac{P_h^\alpha P_h^\beta}{M^2} \equiv \mathcal{Q}^{\alpha\beta}, \tag{28}$$

and $\varepsilon^{\alpha\beta}_{J_z}(P_h)$ is the polarization tensor for $J=2$ bound state and obeys the following set of relations [46,47]

$$\varepsilon^{\alpha\beta}_{J_z}(P_h)=\varepsilon^{\beta\alpha}_{J_z}(P_h),\ \ \varepsilon^{\alpha}_{J_z\alpha}(P_h)=0,\ \ P_{h\alpha}\varepsilon^{\alpha}_{J_z}(P_h)=0,$$
$$\varepsilon^{\mu\nu}_{J_z}(P_h)\varepsilon^{*\alpha\beta}_{J_z}(P_h)=\frac{1}{2}[\mathcal{Q}^{\mu\alpha}\mathcal{Q}^{\nu\beta}+\mathcal{Q}^{\mu\beta}\mathcal{Q}^{\nu\alpha}]-\frac{1}{3}\mathcal{Q}^{\mu\nu}\mathcal{Q}^{\alpha\beta}. \quad (29)$$

The radial wave function $R_0(0)$ and its derivative at origin $R'_1(0)$ are obtained from the LDMEs, and the relations can be found in the Eqs. (36 – 38) within Ref. [27].

The numerical values of LDMEs for these color octet states are extracted from Ref. [48]. Now using the above formalism together with the symmetry relations and sum over the color factors from Ref. [27] in the Eqs. (39,40,43,44,47), we could write the amplitude for color octet states $({}^3S_1, {}^1S_0, {}^3P_{J(0,1,2)})$.

#### 1. $^3S_1$ amplitude

The final expression for the $^3S_1$ scattering amplitude is

$$\mathcal{M}[{}^3S_1^{(8)}](P_h,k)=\frac{1}{4\sqrt{\pi M}}R_0(0)\frac{\sqrt{2}}{2}d_{abc}\times \mathrm{Tr}\left[\sum_{m=1}^{3}O_m(0)(-\not{P}_h+M)\not{\epsilon}^{*}_{s_z}\right], \quad (30)$$

where

$$\sum_{m=1}^{3}O_m(0)=g_s^2(ee_c)\varepsilon^{\rho*}_{\lambda_g}(p_g)\left[\frac{\gamma_\nu(\not{P}h-2\not{q}+M)\gamma_\mu(-\not{P}h-2\not{p}_g+M)\gamma_\rho}{(\hat{s}-M^2)(\hat{u}-M^2)}+\frac{\gamma_\rho(\not{P}h+2\not{p}_g+M)\gamma_\nu(-\not{P}h+2\not{k}+M)\gamma_\mu}{(\hat{s}-M^2)(\hat{t}-M^2)}\right.$$
$$\left.+\frac{\gamma_\nu(\not{P}h-2\not{q}+M)\gamma_\rho(-\not{P}h+2\not{k}+M)\gamma_\mu}{(\hat{t}-M^2)(\hat{u}-M^2)}\right]. \quad (31)$$

Due to the symmetry relations [27] Feynman diagrams 4 and 8 cancel and do not contribute to $^3S_1$ state.

#### 2. $^1S_0$ amplitude

For the $^1S_0$ scattering amplitude the expression reads as

$$\mathcal{M}[{}^1S_0^{(8)}](P_h,k)=\frac{R_0(0)}{4\sqrt{\pi M}}\frac{\sqrt{2}}{2}if_{abc}\mathrm{Tr}[(O_1(0)-O_2(0)-O_3(0)+2O_4(0))(-\not{P}_h+M)\gamma^5], \quad (32)$$

where $O_1(0)$, $O_2(0)$, and $O_3(0)$ are given in Eq. (31) and

$$O_4(0)=g_s^2(ee_c)\varepsilon^{\rho*}_{\lambda_g}(p_g)\frac{\gamma_\nu(\not{P}-2\not{q}+M)\gamma^\sigma}{\hat{u}(\hat{u}-M^2)}\mathcal{T}_{\mu\rho\sigma}(k,p_g). \quad (33)$$

#### 3. $^3P_J$ amplitude

The amplitude for $^3P_J$ can be written as

$$\mathcal{M}[{}^3P_J^{(8)}](P_h,k)=\frac{\sqrt{2}}{2}f_{abc}\sqrt{\frac{3}{4\pi}}R'_1(0)\sum_{L_zS_z}\varepsilon^{\alpha}_{L_z}(P_h)\langle 1L_z;1S_z|JJ_z\rangle\mathrm{Tr}[(O_{1\alpha}(0)-O_{2\alpha}(0)-O_{3\alpha}(0)+2O_{4\alpha}(0))\mathcal{P}_{SS_z}(0)$$
$$+(O_1(0)-O_2(0)-O_3(0)+2O_4(0))\mathcal{P}_{SS_z\alpha}(0)]. \quad (34)$$

### C. $\cos(2\phi_h)$ azimuthal asymmetry

To probe the TMDs in this process, one needs two well-separated scales. While $Q^2$ gives the hard scale, the other scale is given by $P_{h\perp}$, and we consider a kinematical region where the transverse momentum of $J/\psi$ is small compared to the mass of $J/\psi$, $M$ i.e., $P_{h\perp}<M$. For a large transverse momentum of $J/\psi$ collinear factorization is expected to hold. The generic structure of the TMD cross section defined by Eq. (11) is easily obtained from the contraction of the four tensors which are

$$L^{\mu\mu'}(l,q)\Phi^{\nu\nu'}(x,\boldsymbol{k}_\perp)\mathcal{M}^{\gamma^*+g\to J/\psi+g}_{\mu\nu}\mathcal{M}^{*\gamma^*+g\to J/\psi+g}_{\mu'\nu'}. \quad (35)$$

We get a contribution for the amplitude and their corresponding complex conjugate amplitude from all the six states $^1S_0^{(8)}$, $^3S_1^{(1,8)}$, and $^3P^{(8)}_{J(=0,1,2)}$ in the cross section. The summation over the transverse polarization of the final on-shell gluon is given by

$$\sum_{\lambda_a=1}^{2}\varepsilon^{\lambda_a}_{\mu}(p_g)\varepsilon^{*\lambda_a}_{\mu'}(p_g)=-g_{\mu\mu'}+\frac{p_{g\mu}n_{g\mu'}+p_{g\mu'}n_{g\mu}}{p_g\cdot n_g}-\frac{p_{g\mu}p_{g\mu'}}{(p_g\cdot n_g)^2}, \quad (36)$$

with $n^\mu_g=\frac{P^\mu_h}{M}$. In a frame where the virtual photon and target proton move along the $z$-axis, and the lepton scattering plane defines the azimuthal angles $\phi_l=\phi_{l'}=0$, we can write

$$\frac{d^3l'}{(2\pi)^3 2E_{l'}} = \frac{1}{16\pi^2} sydx_B dy, \frac{d^3P_h}{(2\pi)^3 2E_h} = \frac{1}{(2\pi)^3}\frac{1}{2z} dz d^2\mathbf{P}_{h\perp},$$
$$\frac{d^3p_g}{(2\pi)^3 2E_g} = \frac{1}{(2\pi)^3}\frac{1}{2z_2} dz_2 d^2\mathbf{p}_{g\perp}, \tag{37}$$

and the delta function can be written as

$$\delta^4(q + k - P_h - p_g)$$
$$= \delta\left(x - \frac{1}{ys}\left(x_B ys + \frac{M^2 + P_{h\perp}^2}{z} + \frac{(k_\perp - P_{h\perp})^2}{(1-z)}\right)\right)$$
$$\times \frac{2}{ys}\delta(1 - z - z_2) \times \delta^2(\mathbf{k}_\perp - \mathbf{P}_{h\perp} - \mathbf{p}_{g\perp}), \tag{38}$$

where the delta function sets $z_2 = (1 - z)$. After integration over $x$, $z_2$, and $p_{g\perp}$, the final form of the differential cross section can be written as

$$\frac{d\sigma}{dydx_B dz d^2\mathbf{P}_{h\perp}} = \frac{1}{256\pi^4}\frac{1}{x_B^2 s^3 y^2 z(1-z)}\int k_\perp dk_\perp |M'|^2, \tag{39}$$

where $|M'|^2 = \int d\phi |M|^2$, and $k_\perp$ is the magnitude of $\mathbf{k}_\perp$. We only keep the transverse momentum of the initial gluon up to $\mathcal{O}(k_\perp^2/M_p^2)$. We expand in $P_{h\perp}/M$ and keep the terms up to $\mathcal{O}(P_{h\perp}^2/M^2)$. As we are interested in the small-$x$ domain, we have expanded the amplitudes in $x_B$ and did not consider higher-order terms in $x_B$. In [30] where only the CS contributions were considered, the contribution to the asymmetry came from the first Feynman diagram in the numerator and the overlap of the first, second, and third Feynman diagrams in the denominator. Here with the CO contributions included, all the Feynman diagrams contribute.

Thus we could write the final expression for differential scattering cross section as

$$\frac{d\sigma}{dydx_B dz d^2\mathbf{P}_{hT}} = d\sigma^U(\phi_h) + d\sigma^T(\phi_h), \tag{40}$$

where

$$d\sigma^U(\phi_h) = \frac{1}{256\pi^4}\frac{1}{x_B^2 s^3 y^2 z(1-z)}\int k_\perp dk_\perp \{(A_0 + A_1\cos(\phi_h) + A_2\cos(2\phi_h))f_1^g(x, \mathbf{k}_\perp^2)\},$$

and

$$d\sigma^T(\phi_h) = \frac{1}{256\pi^4}\frac{1}{x_B^2 s^3 y^2 z(1-z)}\int dk_\perp \frac{k_\perp^3}{M_p^2}\{(B_0 + B_1\cos(\phi_h) + B_2\cos(2\phi_h))h_1^{\perp g}(x, \mathbf{k}_\perp^2)\}.$$

The analytic expressions of the coefficients $A_0$, $A_1$, $A_2$, $B_0$, $B_1$, and $B_2$ are too lengthy to be given here, so we have not included them in this paper; they are available upon request. The $\cos(2\phi_h)$ asymmetry measured in experiments is defined as

$$\langle\cos(2\phi_h)\rangle = \frac{\int d\phi_h \cos(2\phi_h) d\sigma}{\int d\phi_h d\sigma}, \tag{41}$$

where $\phi_h$ is the azimuthal angle of $J/\psi$ production plane with the lepton plane. The $\cos(2\phi_h)$ asymmetry as a function of $P_{h\perp}, x_B, z$ and $y$ can be written as

$$\langle\cos(2\phi_h)\rangle \propto \frac{\int k_\perp dk_\perp (A_2 f_1^g(x, \mathbf{k}_\perp^2) + \frac{k_\perp^2}{M_p^2} B_2 h_1^{\perp g}(x, \mathbf{k}_\perp^2))}{\int k_\perp dk_\perp (A_0 f_1^g(x, \mathbf{k}_\perp^2) + \frac{k_\perp^2}{M_p^2} B_0 h_1^{\perp g}(x, \mathbf{k}_\perp^2))}. \tag{42}$$

In [30] it was seen that with only the CS contributions in the small-$x$ limit the numerator of the $\cos 2\phi_h$ asymmetry only receives a contribution from the linearly-polarized gluon distributions. Here it is seen that as the CO contributions are included, both the numerator and the denominator of the above asymmetry contain contributions from the unpolarized gluon TMD and the linearly-polarized gluon TMD. Thus in this case, the unpolarized gluon distribution and the linearly-polarized distributions are not disentangled in this process in the kinematics considered. The above asymmetry depends on the ratio of the two and can be used to extract this ratio.

One thing to be noted here is that the $J/\psi$ production in electron-proton collision for a large transverse momentum can be calculated in the collinear factorization approach. For small $P_{h\perp}$, the TMD framework is expected to hold. In the intermediate region, these two results should match. This matching has been shown in [43]. In order to do the matching, one has to evolve the TMDs using TMD evolution [49]. Here, it is necessary to take into account the soft factor that resums the emitted soft gluons. In the final state, the LDMEs need to be modified with the inclusion of the shape function or the smearing functions [50–52]. In [43] one can see that the leading-order contribution in the TMD region, that contributes at $z = 1$ [22],

is matched with the collinear factorized result at large $P_{h\perp}$ with one extra gluon. Here we have extended the calculation in the kinematical region $z < 1$ and small $P_{h\perp}$, where the TMD framework is expected to be valid, and take into account both the CS and CO contributions in the asymmetry.

## III. RESULTS AND DISCUSSION

In this section, we present numerical estimates of the $\cos(2\phi_h)$ asymmetry in the kinematical region to be accessed at the EIC. As gluon TMDs are particularly important in the small-$x$ domain, we are considering the small-$x$ kinematics. At $z = 1$, one gets contribution from the leading order as well as diffractive contributions. Here the momentum fraction of the final gluon is $(1 - z)$. This means as $z \to 1$, the final gluon becomes soft. To keep the final gluon hard, we have imposed a cutoff $z < 0.9$. Also, to avoid the gluon fragmentation contribution to $J/\psi$, we have used a lower cutoff $z > 0.1$. We have checked that changing the lower cutoff does not affect the asymmetry much. We took the mass of the proton to be $M_p = 1$ GeV.

The contraction in the calculation above for the different states i.e., ${}^1S_0^{(8)}$, ${}^3S_1^{(1,8)}$, and ${}^3P_{J(=0,1,2)}^{(8)}$ is calculated using FeynCalc [53,54]. In all the plots of the asymmetry, the long distance matrix elements are taken from Ref. [48] except for the right panel of Fig. 3 and for the plots in Fig. 4, where we have used different sets of LDMEs. The asymmetry depends on the parametrization/model used for the gluon TMDs. In our estimate, we have used two sets of parametrization to calculate the $\cos(2\phi_h)$ asymmetry: 1) Gaussian-type parametrization [20,23,44] for both the unpolarized as well as the linearly-polarized TMDs, and 2) McLerran-Venugopalan (MV) model [55–57] at small-$x$ region.

### A. $\cos(2\phi_h)$ asymmetry in the Gaussian parametrization

In Gaussian type of parametrization, both the TMDs, $f_1^g$ and $h_1^{\perp g}$ are factorized into a product of collinear PDFs times exponential factor which is a function of the transverse momentum

$$f_1^g(x, \mathbf{k}_\perp^2) = f_1^g(x, \mu) \frac{1}{\pi \langle k_\perp^2 \rangle} e^{-k_\perp^2/\langle k_\perp^2 \rangle}, \tag{43}$$

$$h_1^{\perp g}(x, \mathbf{k}_\perp^2) = \frac{M_p^2 f_1^g(x, \mu)}{\pi \langle k_\perp^2 \rangle^2} \frac{2(1-r)}{r} e^{1 - \frac{k_\perp^2}{r\langle k_\perp^2 \rangle}}, \tag{44}$$

$r(0 < r < 1)$ is a parameter. We took the Gaussian width $\langle k_\perp^2 \rangle = 0.25$ GeV$^2$ and $r = 1/3$ in all plots except Fig. 5. The term $f_1^g(x, \mu)$ is the collinear PDF, for which MSTW2008 [58] is used and is probed at the scale $\mu = \sqrt{M^2 + P_{h\perp}^2}$, where $M(= 3.096$ GeV) is the mass of $J/\psi$. The linearly-polarized gluon distribution in the parametrization above satisfies the positivity bound [9], but does not saturate it.

In Figs. 2–5, we have used the Gaussian parametrization of the TMDs. In Figs. 2 and 5 we calculated the total asymmetry by including the contribution from both the color singlet and color octet states in the framework of NRQCD.

In left panel of Fig. 2 we showed the asymmetry as a function of $P_{h\perp}$ at center of mass energy $\sqrt{s} = 100$ GeV and at a fixed value of $Q^2 = 15$ GeV$^2$. The integration ranges are $0.0015 < x_B < 0.1$, $0.1 < z < 0.9$ and $y$ is set by the values of $Q^2$, $s$, and $x_B$. In the right panel of Fig. 2, we showed the asymmetry as a function of $y$ at $\sqrt{s} = 120$ GeV and at fixed $x_B$. The asymmetry is larger for smaller values of $x_B$ and approaches to zero as $y$ tends to 1.

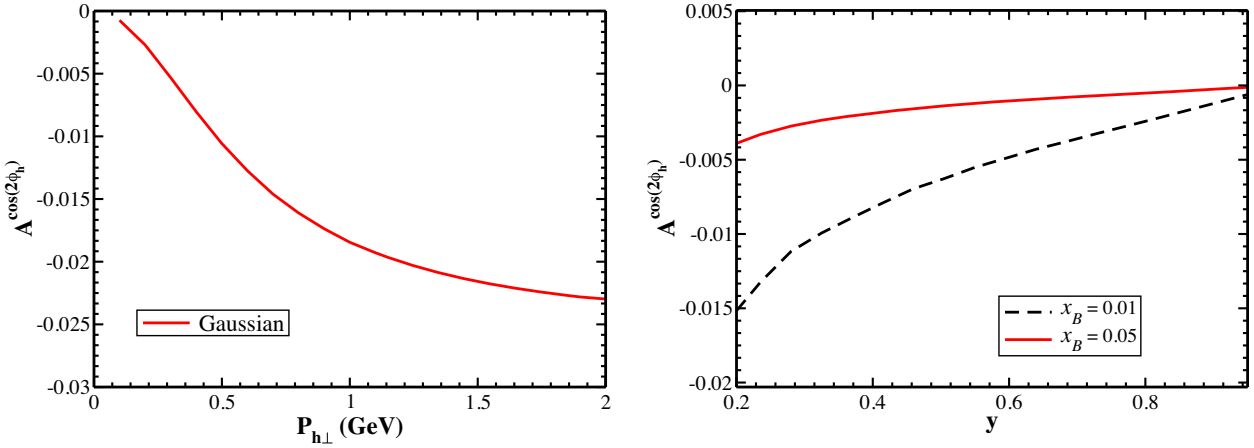


FIG. 2. $\cos(2\phi_h)$ asymmetry in $e + p \to e + J/\psi + X$ process. Left: As a function of $P_{h\perp}$ at $\sqrt{s} = 100$ GeV and $Q^2 = 15$ GeV$^2$. The integration ranges are $0.0015 < x_B < 0.1$, $0.1 < z < 0.9$ and $y$ is set by the values of $Q^2$, $s$, and $x_B$. Right: As a function of $y$ at $\sqrt{s} = 120$ GeV and at fixed $x_B$. The integration ranges are $0 < P_{h\perp} < 2$, $0.1 < z < 0.9$. For both plots CMSWZ set of LDMEs [48] is used.

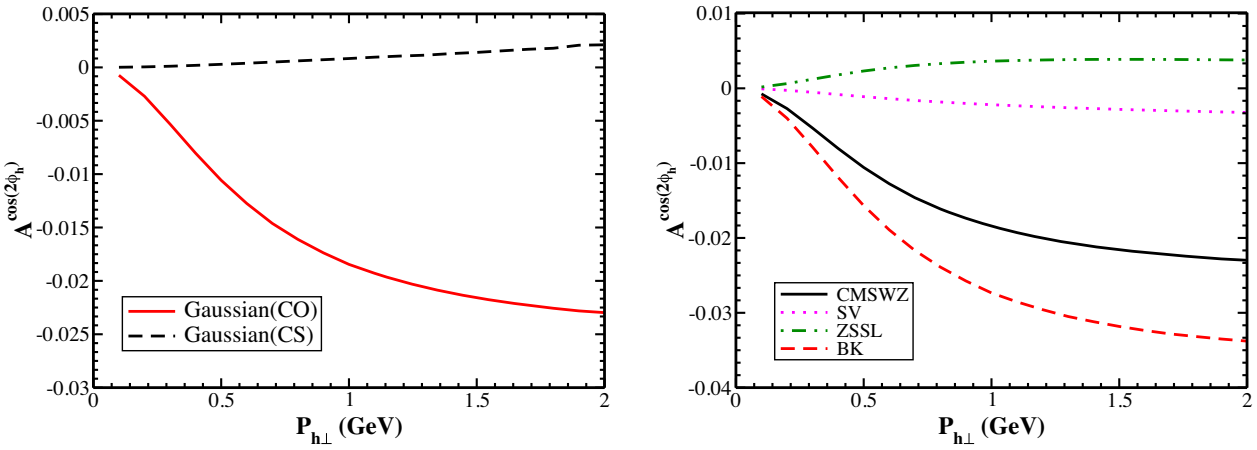


FIG. 3. $\cos(2\phi_h)$ asymmetry in $e + p \to e + J/\psi + X$ process as function of $P_{h\perp}$ at $\sqrt{s} = 100$ GeV and $Q^2 = 15$ GeV$^2$. The integration ranges are $0.0015 < x_B < 0.1$, $0.1 < z < 0.9$ and y is set by the values of $Q^2$, $s$ and $x_B$. Left: contributions from color singlet and color octet states using the LDMEs set CMSWZ [48]. Right: comparing the asymmetry for different LDMEs sets: CMSWZ [48], SV [59], ZSSL [60], BK [61].

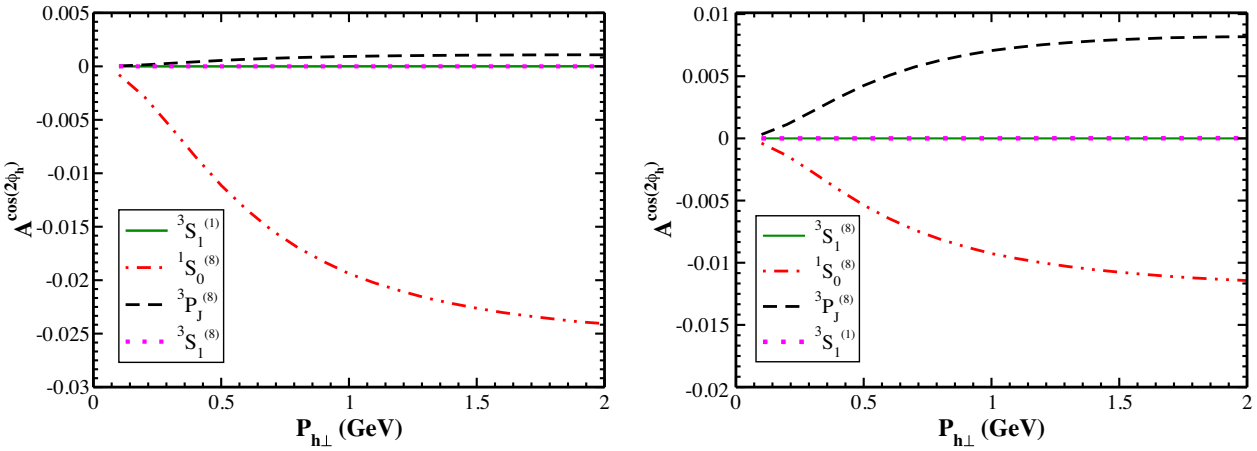


FIG. 4. $\cos(2\phi_h)$ asymmetry in $e + p \to e + J/\psi + X$ process as function of $P_{h\perp}$ at $\sqrt{s} = 100$ GeV and $Q^2 = 15$ GeV$^2$. The integration ranges are $0.0015 < x_B < 0.1$, $0.1 < z < 0.9$ and y is set by the values of $Q^2$, $s$ and $x_B$. Left: asymmetry for the set of LDMEs, CMSWZ [48]. Right: asymmetry for the set of LDMEs SV [59].

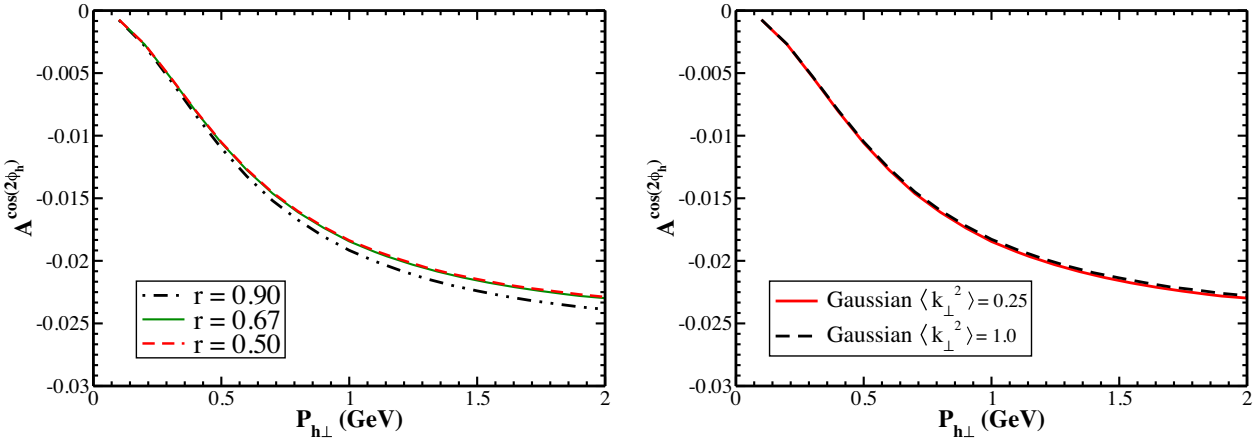


FIG. 5. $\cos(2\phi_h)$ asymmetry in $e + p \to e + J/\psi + X$ process as function of $P_{h\perp}$ at $\sqrt{s} = 100$ GeV and $Q^2 = 15$ GeV$^2$. The integration ranges are $0.0015 < x_B < 0.1$, $0.1 < z < 0.9$ and y is set by the values of $Q^2$, $s$ and $x_B$. Left: asymmetry for three different values of $r$. Right: asymmetry for two different values of Gaussian width parameter. For both plots CMSWZ set of LDMEs [48] is used.

We obtained negative asymmetry which is consistent with the LO calculations shown in [22]. However, the magnitude of the asymmetry is small (only a few percent) even after the CO contributions are included. This could be due to the fact that we have calculated the asymmetry in a particular kinematical region.

In the left panel of Fig. 3, we present the contribution to the asymmetry from the CS and the CO states. From the plot, we see that the color octet states are giving a significant contribution to the asymmetry, whereas the contribution from the CS is almost zero and slightly positive in the higher $P_{h\perp}$ region. In the right panel of Fig. 3, we show the asymmetry for different sets of LDMEs. We see that the magnitude and the sign of the asymmetry depend on the set of LDMEs used. The asymmetry is negative if one uses CMSWZ [48] and BK [61] sets of LDMEs whereas it is smaller and positive for the SV [59] and ZSSL [60] sets. This is because, different states contribute differently depending on the choice of the LDME sets. In the left panel of Fig. 4 we show the contribution coming from all the individual states to the asymmetry for the LDMEs set CMSWZ [48]. For this set of LDMEs, there is a dominance of one single state, $^1S_0^{(8)}$, to the asymmetry, whereas for the LDMEs set SV [59], which is shown in the right panel of the same figure, we have major contributions from two states $^1S_0^{(8)}$ and $^3P_J^{(8)}$. The strong dependence on the magnitude and sign of the asymmetry on the set of LDMEs opens up another interesting possibility of determining these LDMEs using the data from this asymmetry. This could be done by taking ratios of different azimuthal asymmetries or a combination of them, where the dependence on the gluon TMDs cancel out. An investigation in this direction, of determining the LDMEs from azimuthal asymmetries in $J/\psi$ production, has already been reported in [42,28]. We plan to investigate this further in a future publication.

In Fig. 5 we plotted the asymmetry as a function of $P_{h\perp}$ for different values of the parameter $r$ (left) and Gaussian width $\langle k_\perp^2 \rangle$ (right). We do not see any significant change in the asymmetry over different values of Gaussian width and the parameter $r$.

Also, we have checked that there is no significant change in the asymmetry if the value of the center of mass energy is changed for a fixed value of $Q^2$; but the asymmetry decreases with the increase of the $Q^2$ for a fixed value of $s$.

### B. $\cos(2\phi_h)$ asymmetry in the McLerran-Venugopalan model

The McLerran-Venugopalan model [55–57], a classical model, helps us to calculate the gluon distribution in a large nucleus at small $x$. In this model, the Gaussian distribution of color charges is assumed to act like a static source, producing the soft gluons by the Yang-Mills equations. Although originally proposed for a large nucleus, this model has been found to give reasonable phenomenological results in azimuthal asymmetries for a proton in small-$x$ domain [30,36,62]. The analytical expressions for unpolarized and linearly-polarized Weizsäcker-Williams gluon distribution can be written as [63,64]

$$f_1^g(x,\mathbf{k}_\perp^2) = \frac{S_\perp C_F}{\alpha_s \pi^3} \int d\rho \frac{J_0(k_\perp \rho)}{\rho} (1 - \exp^{\frac{-\rho^2}{4} Q_{sg}^2(\rho)}), \quad (45)$$

$$h_1^{\perp g}(x,\mathbf{k}_\perp^2) = \frac{2S_\perp C_F}{\alpha_s \pi^3} \frac{M_P^2}{k_\perp^2} \int d\rho \frac{J_2(k_\perp \rho)}{\rho \log(\frac{1}{\rho^2 \lambda_{\rm QCD}^2})} (1 - \exp^{\frac{-\rho^2}{4} Q_{sg}^2(\rho)}), \quad (46)$$

where $S_\perp$ is the transverse size of the proton, $Q_{sg}(\rho)$ is the saturation scale for gluons, which in general is a function of $x$ but in the MV model depends on dipole

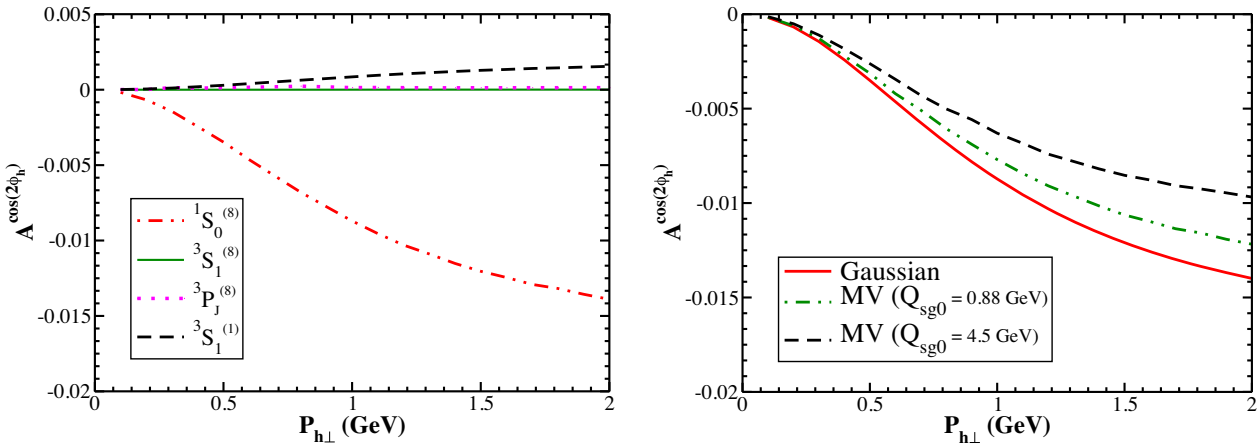


FIG. 6. $\cos(2\phi_h)$ asymmetry in $e + p \to e + J/\psi + X$ process as function of $P_{h\perp}$ at $\sqrt{s} = 150$ GeV, $x = 0.01$ and $z = 0.7$. Left: contribution to the $\cos(2\phi)$ asymmetry coming from the individual states, as a function of $P_{h\perp}$ in the NRQCD framework using the color octet model. Right: comparison of the Gaussian and MV model (with two different values of $Q_{sg0}$). For both plots, CMSWZ set of LDMEs [48] is used.

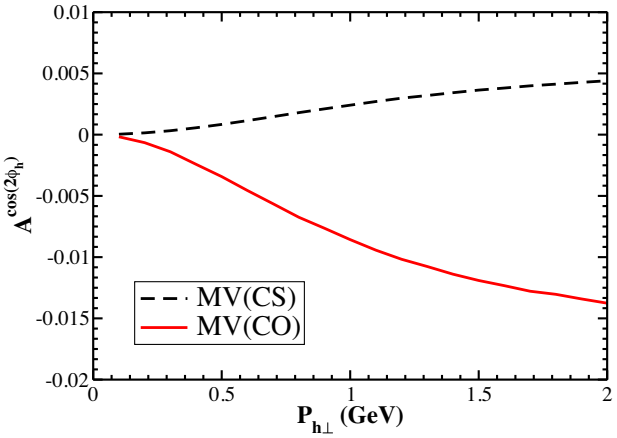


FIG. 7. $\cos(2\phi_h)$ asymmetry in $e + p \to e + J/\psi + X$ process as function of $P_{h\perp}$ at $\sqrt{s} = 150$ GeV, $x = 0.01$ and $z = 0.7$. Contribution to the $\cos(2\phi_h)$ asymmetry coming from the color singlet and color octet models. CMSWZ set of LDMEs [48] is used.

size $\rho$ logarithmically. Here $Q_{sg}^2(\rho) = Q_{sg0}^2 \ln(1/\rho^2\lambda^2 + \epsilon)$, where $Q_{sg0}^2 = (N_c/C_F)Q_{s0}^2$ with $Q_{s0}^2 = 0.35$ GeV$^2$ at $x = x_0 = 10^{-2}$ and $\lambda_{\rm QCD} = 0.2$ GeV from the HERA data [65] fitting. Following the approach of [62], a regulator $\epsilon$ is added for numerical convergence. The results for the MV parametrization are obtained in the kinematic region defined by $\sqrt{s} = 150$ GeV, $x = 0.01$ and $z = 0.7$. The integration ranges are $y \in [0.2, 0.9]$ and $x_B \in [0.005, 0.009]$. The value of $Q$ is set according to $y, x_B$, and $s$. In Fig. 6 (left), we present the contribution to the $\cos(2\phi_h)$ asymmetry for the $J/\psi$ coming from the individual states, as a function of $P_{h\perp}$. The maximum contribution to the asymmetry comes from the ${}^1S_0^{(8)}$ state. In the same Fig. 6 (right) we show the comparison of the asymmetry in the Gaussian and the MV model, respectively (with two different values of $Q_{sg0}$ [65,66]) within the same kinematical region as discussed above. The asymmetry in the MV model depends on the saturation scale. We note that the Gaussian parametrization of the TMDs gives larger $\cos(2\phi_h)$ asymmetry. In Fig. 7 we compare the contribution to the asymmetry from color singlet and color octet states. We find that a larger contribution to the $\cos(2\phi_h)$ asymmetry comes from color octet states, which is negative. Color singlet states give a small positive contribution to the asymmetry.

## IV. CONCLUSION

In this article, we have studied the $\cos(2\phi_h)$ asymmetry in $J/\psi$ production in an electron-proton collision in the kinematics of the future electron-ion collider. We calculated them in the small-$x$ domain, where the gluon TMDs, namely the unpolarized and linearly-polarized gluon TMDs are important in unpolarized scattering. The dominant subprocess in this kinematical region for $J/\psi$ production is the virtual-photon-gluon fusion process $\gamma^* + g \to J/\psi + g$. We used the NRQCD based color octet formalism for calculating the $J/\psi$ production rate. The $\cos(2\phi_h)$ asymmetry within the considered kinematic region is small but it can be detected at the planned EIC. The asymmetry depends on the parametrization of the gluon TMDs used. We used both the Gaussian as well as the MV model for the parametrization. The magnitude of the asymmetry is found to be larger for Gaussian parametrization. We have included contributions both from CO as well as CS states. Overall, our calculation shows that the $\cos(2\phi_h)$ asymmetry in $J/\psi$ production could be a useful tool to probe the ratio of the linearly-polarized gluon TMD and the unpolarized gluon TMD in the small-$x$ region at the EIC. The magnitude and the sign of the asymmetry depends on the LDMEs used, in fact this gives the possibility to shed light on the LDMEs using data from this asymmetry; for example by taking combinations of azimuthal asymmetries where the dependence on the TMDs cancel out. We plan to investigate this issue more in another publication. In particular, contributions from individual states are found to depend substantially on the set of LDMEs used.

[1] J. P. Ralston and D. E. Soper, Nucl. Phys. **B152**, 109 (1979).
[2] J. C. Collins and D. E. Soper, Nucl. Phys. **B193**, 381 (1981).
[3] J. C. Collins, D. E. Soper, and G. Sterman, Nucl. Phys. **B250**, 199 (1985).
[4] J. C. Collins, D. E. Soper, and G. Sterman, Phys. Lett. **126B**, 275 (1983).
[5] D. Boer and P. Mulders, Nucl. Phys. **B569**, 505 (2000).
[6] M. Arneodo, A. Arvidson, J. Aubert, B. Badelek, J. Beaufays, C. Bee, C. Benchouk, G. Berghoff, I. Bird, D. Blum *et al.*, Z. Phys. C **34**, 277 (1987).
[7] A. Airapetian, N. Akopov, Z. Akopov, M. Amarian, A. Andrus, E. Aschenauer, W. Augustyniak, R. Avakian, A. Avetissian, E. Avetissian *et al.*, Phys. Rev. Lett. **94**, 012002 (2005).
[8] A. Airapetian *et al.* (The HERMES Collaboration), Phys. Rev. Lett. **84**, 4047 (2000).
[9] P. Mulders and J. Rodrigues, Phys. Rev. D **63**, 094021 (2001).
[10] M. Buffing, A. Mukherjee, and P. Mulders, Phys. Rev. D **88**, 054027 (2013).

[11] Y. V. Kovchegov and A. H. Mueller, Nucl. Phys. **B529**, 451 (1998).
[12] L. D. McLerran and R. Venugopalan, Phys. Rev. D **59**, 094002 (1999).
[13] F. Dominguez, J.-W. Qiu, B.-W. Xiao, and F. Yuan, Phys. Rev. D **85**, 045003 (2012).
[14] D. Boer, W. J. den Dunnen, C. Pisano, M. Schlegel, and W. Vogelsang, Phys. Rev. Lett. **108**, 032002 (2012).
[15] P. Sun, B.-W. Xiao, and F. Yuan, Phys. Rev. D **84**, 094005 (2011).
[16] J.-W. Qiu, M. Schlegel, and W. Vogelsang, Phys. Rev. Lett. **107**, 062001 (2011).
[17] G.-P. Zhang, Phys. Rev. D **90**, 094011 (2014).
[18] D. Boer and C. Pisano, Phys. Rev. D **91**, 074024 (2015).
[19] D. Boer and W. J. den Dunnen, Nucl. Phys. **B886**, 421 (2014).
[20] A. Mukherjee and S. Rajesh, Phys. Rev. D **93**, 054018 (2016).
[21] M. G. Echevarria, T. Kasemets, P. J. Mulders, and C. Pisano, J. High Energy Phys. 07 (2015) 158.
[22] A. Mukherjee and S. Rajesh, Eur. Phys. J. C **77**, 854 (2017).
[23] A. Mukherjee and S. Rajesh, Phys. Rev. D **95**, 034039 (2017).
[24] D. Boer, Few-Body Syst. **58**, 32 (2017).
[25] J.-P. Lansberg, C. Pisano, and M. Schlegel, Nucl. Phys. **B920**, 192 (2017).
[26] U. D'Alesio, F. Murgia, C. Pisano, and P. Taels, Phys. Rev. D **96**, 036011 (2017).
[27] S. Rajesh, R. Kishore, and A. Mukherjee, Phys. Rev. D **98**, 014007 (2018).
[28] A. Bacchetta, D. Boer, C. Pisano, and P. Taels, Eur. Phys. J. C **80**, 1 (2020).
[29] J.-P. Lansberg, C. Pisano, F. Scarpa, and M. Schlegel, Phys. Lett. B **784**, 217 (2018).
[30] R. Kishore and A. Mukherjee, Phys. Rev. D **99**, 054012 (2019).
[31] P. Sun, C.-P. Yuan, and F. Yuan, Phys. Rev. D **88**, 054008 (2013).
[32] J. Ma, J. Wang, and S. Zhao, Phys. Rev. D **88**, 014027 (2013).
[33] J. Ma, J. Wang, and S. Zhao, Phys. Lett. B **737**, 103 (2014).
[34] D. Boer, P. J. Mulders, C. Pisano, and J. Zhou, J. High Energy Phys. 08 (2016) 001.
[35] D. Boer, S. J. Brodsky, P. J. Mulders, and C. Pisano, Phys. Rev. Lett. **106**, 132001 (2011).
[36] C. Pisano, D. Boer, S. J. Brodsky, M. G. Buffing, and P. J. Mulders, J. High Energy Phys. 10 (2013) 024.
[37] W. J. Den Dunnen, J.-P. Lansberg, C. Pisano, and M. Schlegel, Phys. Rev. Lett. **112**, 212001 (2014).
[38] A. Efremov, N. Y. Ivanov, and O. Teryaev, Phys. Lett. B **777**, 435 (2018).
[39] A. Efremov, N. Y. Ivanov, and O. Teryaev, Phys. Lett. B **780**, 303 (2018).
[40] J.-P. Lansberg, Phys. Rep. **889**, 1 (2020).
[41] F. Cooper, M. X. Liu, and G. C. Nayak, Phys. Rev. Lett. **93**, 171801 (2004).
[42] D. Boer, C. Pisano, and P. Taels, Phys. Rev. D **103**, 074012 (2021).
[43] D. Boer, U. D'Alesio, F. Murgia, C. Pisano, and P. Taels, J. High Energy Phys. 09 (2020) 040.
[44] D. Boer and C. Pisano, Phys. Rev. D **86**, 094007 (2012).
[45] R. Baier and R. Rückl, Z. Phys. C **19**, 251 (1983).
[46] J. H. Kühn, J. Kaplan, and E. G. O. Safiani, Nucl. Phys. **B157**, 125 (1979).
[47] B. Guberina, J. Kühn, R. D. Peccei, and R. Rückl, Nucl. Phys. **B174**, 317 (1980).
[48] K.-T. Chao, Y.-Q. Ma, H.-S. Shao, K. Wang, and Y.-J. Zhang, Phys. Rev. Lett. **108**, 242004 (2012).
[49] S. M. Aybat and T. C. Rogers, Phys. Rev. D **83**, 114042 (2011).
[50] S. Fleming, A. K. Leibovich, and T. Mehen, Phys. Rev. D **68**, 094011 (2003).
[51] M. G. Echevarria, J. High Energy Phys. 10 (2019) 144.
[52] S. Fleming, Y. Makris, and T. Mehen, J. High Energy Phys. 04 (2020) 122.
[53] V. Shtabovenko, R. Mertig, and F. Orellana, Comput. Phys. Commun. **256**, 107478 (2020).
[54] R. Mertig, M. Böhm, and A. Denner, Comput. Phys. Commun. **64**, 345 (1991).
[55] L. McLerran and R. Venugopalan, Phys. Rev. D **49**, 2233 (1994).
[56] L. McLerran and R. Venugopalan, Phys. Rev. D **49**, 3352 (1994).
[57] L. McLerran and R. Venugopalan, Phys. Rev. D **50**, 2225 (1994).
[58] A. D. Martin, W. J. Stirling, R. S. Thorne, and G. Watt, Eur. Phys. J. C **63**, 189 (2009).
[59] R. Sharma and I. Vitev, Phys. Rev. C **87**, 044905 (2013).
[60] H.-F. Zhang, Z. Sun, W.-L. Sang, and R. Li, Phys. Rev. Lett. **114**, 092006 (2015).
[61] M. Butenschoen and B. A. Kniehl, Phys. Rev. D **84**, 051501 (2011).
[62] U. D'Alesio, F. Murgia, C. Pisano, and P. Taels, Phys. Rev. D **100**, 094016 (2019).
[63] A. Metz and J. Zhou, Phys. Rev. D **84**, 051503 (2011).
[64] F. Dominguez, J.-W. Qiu, B.-W. Xiao, and F. Yuan, Phys. Rev. D **85**, 045003 (2012).
[65] K. Golec-Biernat and M. Wüsthoff, Phys. Rev. D **59**, 014017 (1998).
[66] J. Albacete, N. Armesto, J. Milhano, C. Salgado, and U. Wiedemann, Phys. Rev. D **71**, 014003 (2005).